

# Genuinely Multidimensional Kinetic Scheme For Euler Equations

Praveer Tiwari<sup>1</sup>, SV Raghurama Rao<sup>2</sup>

1. Department of Physics, Indian Institute of Science, Bangalore

2. Department of Aerospace Engineering, Indian Institute of Science, Bangalore

---

## Abstract

A new framework based on Boltzmann equation which is genuinely multidimensional and mesh-less is developed for solving Euler's equations. The idea is to use the method of moment of Boltzmann equation to operate in multidimensions using polar coordinates. The aim is to develop a framework which is genuinely multidimensional and can be implemented with different methodologies, no matter whether it is in finite difference, finite volume or finite element form. There is a considerable improvement in capturing shocks and other discontinuities. Also, since the method is multidimensional, the flow features are captured isotropically. The method is further extended to second order using 'Arc of Approach' concept. The framework is developed as a finite difference method (called as GINEUS) and is tested on the benchmark test cases. The results are compared against Kinetic Flux Vector Splitting Method.

---

## 1. Introduction

With the emergence of Godunov's scheme (Godunov [12]), the quest for finding scheme to resolve shocks and other discontinuities for hyperbolic gas dynamic equations had started. What followed are several central and upwind discretization methods, of which, schemes by Leer [20], Osher and Solomon [30] and Lax and Wendroff [19] are some of the prominent ones. A feat of exact shock capturing in 1D is achieved in the schemes by Roe [40], Liou [24](AUSM+) and Jaisankar and Rao [14](MOVERS) of which AUSM+ also achieves exact contact discontinuity capturing. Although, these schemes were efficient, robust and accurate in 1D, their 2D counterparts were not accurate in resolving flow features because they were modelling waves propagating along the grid. Physically, the waves can propagate in any direction, so splitting it along grid axes becomes meaningless. Hence, it was realized that there is a need of a new framework which could account for the wave propagation in multidimensions. This led to development of a new class of schemes which are genuinely multidimensional that can resolve shocks and other discontinuities even when they are not aligned to grids.

Several attempts have been made to eliminate the grid dependence for capturing flow features. P.L.Roe [34] laid the foundation of this class of schemes by introducing fluctuation splitting method which was based on the idea that the solution assumes piecewise continuous solution inside a cell, contrary to Godunov's framework. This work was further developed to propose a method (Roe [41]) where the multidimensional Euler equations are modified, in a similar way as it was done for the Riemann solver (Roe [40]), to simpler components. Hirsch et al. [13] introduced a scheme in which they diagonalized the Euler equations using the local wave propagation direction coming from pressure gradient and stress tensor. This way upwinding is done based on local flow features which is independent of the background grid. Building on this idea, Powell and van Leer [35] introduced genuinely multidimensional cell-vertex scheme in which data is decomposed into four variables which is then convected to appropriate directions using cell vertex scheme. Parpia and Michalek [31] introduced a scheme based on the assumption of three waves at each interface where the direction and strength of these waves are determined by local flow features. Colella [7] introduced a multidimensional scheme where numerical fluxes are evaluated based on characteristic form of multidimensional Euler equation at the interface. Dadone and Bernard [8] introduced a scheme based on flux-difference splitting, at each face, along two perpendicular direction where the directions are chosen based on pressure gradient at the face. Roe came back with another idea (Roe and Deconinck [42]) where linear wave solutions are obtained from the piecewise linear data over the cell (which is the enclosure of the data points) and hence avoiding the need of flow variables at the cell interfaces. Parpia and Michalek [32], introduced yet another scheme which extracts the information about the waves using reconstruction procedure applied on the data present at the vertices of a triangle. Abgrall [1] came up with a scheme involving linearization of Euler equation whose exact solution is then used for evaluating the flux at the interfaces in multidimensional way. Deconinck et al. [9] devised a multidimensional scheme based

on fluctuation-splitting scheme introduced by P.L.Roe [34]. Later that year, Eppard and Grossman took Deconinck's idea to Boltzmann level. They used fluctuation splitting of distribution function at kinetic level thereby obtaining the fluctuations in conserved variables as its moments. LeVeque [22] introduced a class of high resolution multidimensional schemes based on solving Riemann problems and using limiters to get the resulting waves which is then propagated in multidimensions. Kurganov and Petrova [17] introduced yet another genuinely multidimensional scheme using precise information about the local speeds of propagation in his high resolution central scheme Kurganov and Tadmor [18]. Rao and Rao [38] introduced framework which involved using relaxation schemes combined with splitting method to linearize the non linear hyperbolic conservation equation followed by tracing the foot of the characteristic of the resulting equation to get the genuinely multidimensional structure. Kissmann et al. [16] extended this idea to arbitrary orthogonal grids. Lukacova coupled finite volume formulation with operators constructed using bicharacteristics of the multidimensional hyperbolic system constrained to capture the wave propagation in arbitrary direction ( Lukacova-Medvid'ova et al. [27] and Lukacova-Medvid'ova et al. [26]). Later, Arun et al. [2] extended this idea to hyperbolic systems for spatially varying flux functions. Rossmannith [43] extended Leveque and Pelanti's idea (LeVeque and Pelanti [21]) to construct a multidimensional relaxation system to obtain multidimensional approximate Riemann solvers. Razavi et al. [39] extracted the multidimensional characteristic structure of incompressible flows, modified by artificial compressibility, to construct inherent multidimensional upwind scheme. Balsara [4] introduced a multidimensional Riemann solver that takes input from neighbouring points for getting fluxes in a way which creates self-similar strongly interacting one dimensional Riemann problem. Initially, the scheme was restricted to use only HLLC Riemann solver, but later he himself developed it to work with any 1D self-similar Riemann solver in structured and unstructured mesh (Balsara [5] and Balsara and Dumbser [6] respectively). Next on the list comes Mishra and Tadmor [29], who reformulated finite volume scheme in terms of vertex centered numerical potentials to get a genuinely multidimensional structure. One of the recent is by K.R Arun and M. Lukacova-Medvid'ova (3) where they work in DVBE framework and isotropically cover the domain by foot of the characteristic. Jaisankar and Sheshadri [15] used direction based diffusion regulator with dimension splitting solvers to moderate the excess multidimensional diffusion.

Instead of introducing a new framework to model multidimensionality of waves, the innate nature of method of moments of Boltzmann equation can be exploited to capture waves in multidimensions. This feature has been explored by Rao and Deshpande [37] where he used rotational coordinates to take moments of the Boltzmann equation while coupling the upwinding with the direction of microscopic flow velocity. Although, this was a good attempt to extract the genuinely multidimension nature of kinetic framework, the absence of closed form expressions for the integral meant that scheme would have to depend upon numerical quadrature which was costly. The present work aims to re-introduce the idea in a way which is computationally inexpensive and technically more obvious. The aim of the paper is to introduce the idea in upwind framework.

Next section explains briefly, the method of moments of Boltzmann equation to obtain Euler equations. The following sections will introduce the first order formulation of the idea, the second order extension and ultimately the last section will give the numerical results for the standard test cases.

## 2. Euler Equations from Boltzmann Equation

The Boltzmann Equation, given by (1), has proved to be useful tool in analysis of macroscopic fluid flows.

$$\frac{\partial f}{\partial t} + \mathbf{v} \cdot \vec{\nabla}_x f + \mathbf{a} \cdot \vec{\nabla}_v f = J(\mathbf{x}, \mathbf{v}, t) \quad (1)$$

where  $f$  is the probability distribution function,  $\mathbf{v} = (v_x, v_y, v_z)$ ,  $\mathbf{a}$  is the acceleration due to external forces and  $J$  is the collision term. In this section, we will briefly discuss about obtaining Euler Equation (inviscid form of N-S E) from Boltzmann Equation. Consider equation (1) and the vector

$$\psi = \left\{ \begin{array}{c} 1 \\ v_x \\ v_y \\ v_z \\ I + \frac{1}{2}(v_x^2 + v_y^2 + v_z^2) \end{array} \right\}. \quad (2)$$

Taking moment of (1) with  $\psi$ , we have

$$\langle \psi, \frac{\partial f}{\partial t} + \mathbf{v} \cdot \vec{\nabla}_x f + \mathbf{a} \cdot \vec{\nabla}_v f = J(\mathbf{x}, \mathbf{v}, t) \rangle \quad (3)$$

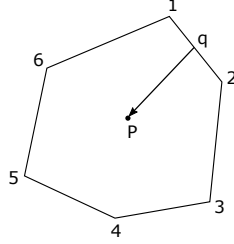


Figure 1: Central point P with all the neighbouring points.

It is assumed that the collisions between fluid molecules at microscopic level are perfectly elastic so that the collision integral conserves mass, momentum and energy. Secondly, it is assumed that there is no external forces acting on the system which removes the third term on the right hand side of equation 1. In this setup, system relaxes to Maxwellian distribution, given by

$$f^M = \rho \left( \frac{\beta}{\pi I_0} \right)^{\frac{D}{2}} e^{-\beta \Sigma^D (v_i - u_i)^2 - \frac{I}{I_0}}, \quad (4)$$

where  $\beta = 1/2RT$ ,  $D$  is the spatial dimension of the fluid flow and  $I$  is the internal energy. Accounting for these two assumptions, the moment equation reads:

$$\langle \psi, \frac{\partial f}{\partial t} + \mathbf{v} \cdot \vec{\nabla}_x f = 0, f = f^M \rangle. \quad (5)$$

The above equation boils down to

$$\frac{\partial U}{\partial t} + \frac{\partial G_1}{\partial x} + \frac{\partial G_2}{\partial y} + \frac{\partial G_3}{\partial z} = 0, \quad (6)$$

where

$$U = \begin{Bmatrix} \rho \\ \rho u_x \\ \rho u_y \\ \rho u_z \\ \rho E \end{Bmatrix}, G_1 = \begin{Bmatrix} \rho u_x \\ P + \rho u_x^2 \\ \rho u_x u_y \\ \rho u_x u_z \\ \rho u_x E \end{Bmatrix}, G_2 = \begin{Bmatrix} \rho u_y \\ \rho u_x u_y \\ P + \rho u_y^2 \\ \rho u_y u_z \\ \rho u_y E \end{Bmatrix}, G_3 = \begin{Bmatrix} \rho u_z \\ \rho u_x u_z \\ \rho u_y u_z \\ P + \rho u_z^2 \\ \rho u_z E \end{Bmatrix}, \quad (7)$$

$E = e + \sum_{i=x,y,z} (u_i^2/2)$  and  $e = P/\rho(\gamma - 1)$ .

The hyperbolic system (6) represents the well-known Euler equations of Gas Dynamics. In 2D, it boils down to

$$\frac{\partial U}{\partial t} + \frac{\partial G_1}{\partial x} + \frac{\partial G_2}{\partial y} = 0, \quad (8)$$

where

$$U = \begin{Bmatrix} \rho \\ \rho u_x \\ \rho u_y \\ \rho E \end{Bmatrix}, G_1 = \begin{Bmatrix} \rho u_x \\ P + \rho u_x^2 \\ \rho u_x u_y \\ \rho u_x E \end{Bmatrix}, G_2 = \begin{Bmatrix} \rho u_y \\ \rho u_x u_y \\ P + \rho u_y^2 \\ \rho u_y E \end{Bmatrix}. \quad (9)$$

### 3. Grid Independent Essentially Upwinding Scheme

The present scheme basically does upwinding at microscopic level based on particle velocity. It is an ingenious extension, in some sense, of the grid-aligned kinetic theory based upwind method (KFVS). We have a central point P whose value has to be updated in time. The neighbours around the central point P are provided (as shown in the figure (1)).

Consider the face RS such that R and S are in the set of data points of the neighbourhood of P.

The flux term of the Boltzmann equation is given by :

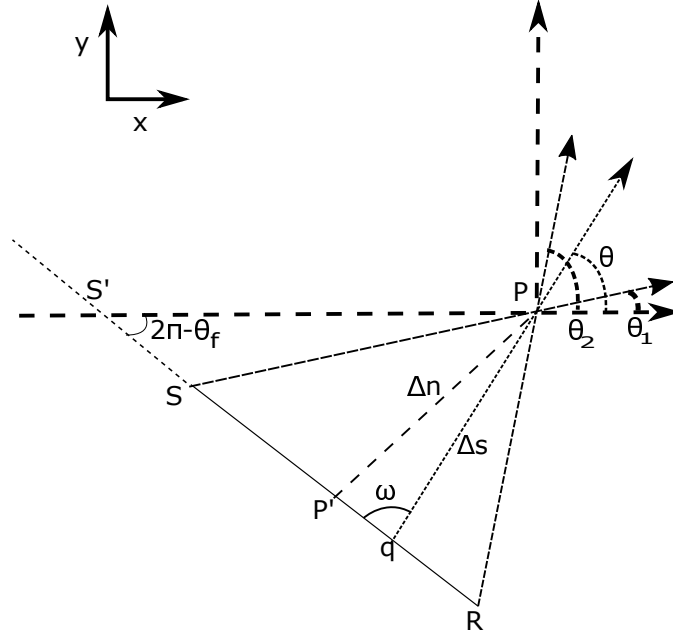


Figure 2: Upwinding in Multidimensions.

$$\vec{v} \cdot \nabla_x f = v \frac{\partial f}{\partial s}, \quad (10)$$

where  $\hat{s}$  is the direction of velocity  $\vec{v}$ . The above equation can be proved in two steps. First note that dot product is a scalar and hence is invariant under rotation of coordinate axes. In the second step, choose the coordinate axes such that one of the axis is parallel to  $\vec{v}$ .

### 3.1. First Order Formulation

Equation (10) can be approximated as following:

$$v \frac{\partial f}{\partial s} \simeq v \frac{\Delta f}{\Delta s} \quad (11)$$

or

$$v \frac{\Delta f}{\Delta s} = v \frac{\Delta f}{\Delta n} |\sin \omega| \quad (12)$$

Since polar coordinates is being used, the moment vector is written as:

$$\psi = \begin{pmatrix} 1 \\ v \cos \theta \\ v \sin \theta \\ I + \frac{1}{2} v^2 \end{pmatrix} \quad (13)$$

Using equation (5), moment equation reads

$$\langle \psi, v \frac{\partial f}{\partial s}, f = f^M \rangle \simeq \int_0^\infty \int_0^{2\pi} \psi v^2 \left[ \frac{f_p^M - f_q^M}{\Delta n} \right] \sin \omega \, dv d\theta \quad (14)$$

Note that we have already integrated out internal energy because it has very little role to play in upwinding.

The next step is to construct a polygon with neighboring points as its vertices. Then, the above integral can be written as the summation of integrals along different edges. Equation (14), then, reads as:

$$\langle \psi, v \frac{\partial f}{\partial s}, f = f^M \rangle \simeq \sum_{\text{all edges}} \int_0^{\theta_{2,edge}} \int_{\theta_{1,edge}} \psi v^2 \frac{f_p^M - f_q^M}{\Delta n} \sin \omega \, dv d\theta \quad (15)$$

where  $\theta_{1,edge}$  and  $\theta_{2,edge}$  are the starting and ending angle (going anticlockwise) of the edge, when measured with center point as origin. The expression for  $f_q^M$  as a function of the polar angle can be obtained by doing linear interpolation of the distribution function along the edge under consideration. So  $f_q^M$  can be written as:

$$f_q^M = D_1(\theta)f_R^M + D_2(\theta)f_S^M \quad (16)$$

where  $R$  and  $S$  are the vertices corresponding to the given edge. The expressions for  $D_1(\theta)$  and  $D_2(\theta)$  are derived in Appendix. Finally, note that the integral given by (15) has no closed form solution for Maxwellian distribution of velocity at equilibrium. This means that, to solve (15), numerical quadrature has to be used. This problem can be avoided by noting the work of Sanders and Prendergast [44], in which he used combinations of Dirac-delta function at different points. In other words, Maxwellian can be approximated by 5 beams (for 2-D and 7 beams in 3-D). More precisely it is written as

$$f^M \simeq e^{-\frac{I}{v_0}} (a\delta(v_1 - u_1)\delta(v_2 - u_2) + b \sum_{(u^{(1)}, u^{(2)}) \in \Omega} (\delta(v_1 - u^{(1)})\delta(v_2 - u^{(2)})) \quad (17)$$

where  $\Omega = \{(u_1, u_2), (u_1, u_2 \pm \Delta u), (u_1 \pm \Delta u, u_2)\}$ . Call this approximate function  $f^B$ . The values of  $a$ ,  $b$  and  $\Delta u$  are derived by ensuring that it gives correct moments (Appendix).

Using this, the semi-discrete equation is given by:

$$\frac{\partial U}{\partial t} = \sum_{all\ edges} \frac{1}{\Delta n_{RS}} \int_0^{\theta_{2,RS}} \int_{\theta_{1,RS}} \psi v^2 \sin\alpha (D_1(\theta)f_R^B + D_2(\theta)f_S^B - f_p^B) dv d\theta \quad (18)$$

The above integral for each edge of the sum contains 15 integrals (3 distribution functions with 5 beams each) of the form

$$\int_0^{\theta_{2,RS}} \int_{\theta_{1,RS}} \frac{\psi v^2 \times D(\theta) \times c \times \sin\alpha \times \delta(v \cos\theta - u^{(1)})\delta(v \sin\theta - u^{(2)})}{\Delta n_{RS}} dv d\theta, \quad (19)$$

where  $D(\theta) = -1$  for  $f_p^B$ ;  $D_1(\theta)$  for  $f_R^B$  and  $D_2(\theta)$  for  $f_S^B$ . Similarly,  $c = a$  or  $b$ , depending on whether it is a central beam or a side beam. And  $(u^{(1)}, u^{(2)}) = (u_1, u_2)$  or  $(u_1, u_2 \pm \Delta u)$  or  $(u_1 \pm \Delta u, u_2)$  depending on the beam being evaluated.

Integral (19) comes out to be

$$I = \begin{cases} \frac{\phi q D(\theta_0) c \sin\omega}{\Delta n_{RS}} & \theta_{1,RS} < \theta_0 < \theta_{2,RS} \\ 0 & otherwise \end{cases}, \quad (20)$$

where  $q = \sqrt{(u^{(1)})^2 + (u^{(2)})^2}$ ,  $\theta_0$  is the angle made  $(u^{(1)}, u^{(2)})$  with positive x-axis and

$$\phi = \begin{Bmatrix} 1 \\ u^{(1)} \\ u^{(2)} \\ I + \frac{1}{2}q^2 \end{Bmatrix}. \quad (21)$$

### 3.2. Second Order Formulation

In this section the formulation given in section 3.1 is extended to second order. From(10), we have

$$\vec{v} \cdot \nabla_x f = v \frac{\partial f}{\partial s} \quad (22)$$

For doing second order approximation of  $\frac{\partial f}{\partial s}$ , 5 point stencil is required in each direction. The concept ‘‘Arc of Approach’’ is introduced for getting the same. The idea is to use the second order discretization of linear convection equation and apply it to the Boltzmann equation which has been reduced to one dimension by equation (10).

The 1D linear convection equation is given by

$$u_t + au_x = 0 \quad a > 0. \quad (23)$$

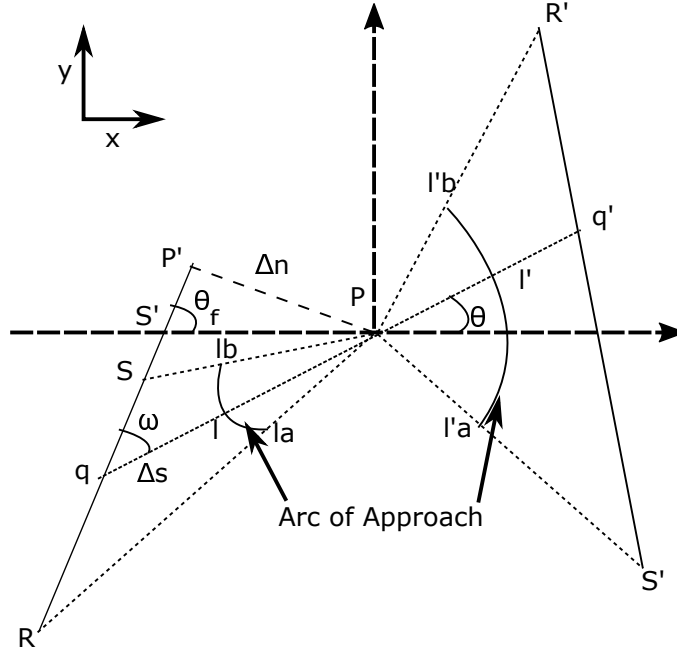


Figure 3: Showing different interpolations required for the Arc of Approach method.

The update formula according to common framework for looking at limiters given by Sweby [46], reads

$$u_i^{n+1} = u_i^n - \lambda(u_i - u_{i-1}) - (\psi_i F_{i+1/2} - \psi_{i-1} F_{i-1/2}) \quad (24)$$

where  $\lambda = \frac{a\Delta t}{\Delta x}$ ,

$$F_{i+1/2} = \frac{1}{2}\lambda(1 - \lambda)(u_{i+1} - u_i) \quad (25)$$

and

$$\psi_i = \psi(R_i) = \psi\left(\frac{u_{i+1} - u_i}{u_i - u_{i-1}}\right) \quad (26)$$

is the limiter function.

Since Boltzmann equation is also being discretized in one direction, its update formula for the second order extension can be written in the form of 24 . The central point P assumes the role of  $i$  and all other points are assigned along the line segment  $qPq'$ .

The fully discretized update formula (following equation (24)), is then given by

$$f_P^{n+1} = f_P^n - \frac{1}{2} \left[ \frac{2v\Delta t}{\Delta s} (f_P - f_l) + F_{l'P} - F_{Pl} \right], \quad (27)$$

where

$$F_{l'P} = \psi_P \left( \frac{v\Delta t}{\Delta s'} \right) \left( 1 - \frac{v\Delta t}{\Delta s'} \right) (f_{l'} - f_P) \quad (28)$$

and

$$F_{Pl} = \psi_l \left( \frac{v\Delta t}{\Delta s} \right) \left( 1 - \frac{v\Delta t}{\Delta s} \right) (f_P - f_l), \quad (29)$$

where

$$\psi_P = \psi(R_P) = \psi\left(\frac{\rho_{l'} - \rho_P}{\rho_P - \rho_l}\right) \quad (30)$$

and

$$\psi_l = \psi(R_l) = \psi\left(\frac{\rho_P - \rho_l}{\rho_l - \rho_q}\right). \quad (31)$$

Finally, the distribution function at the point  $l$  and  $l'$  can be obtained by aforementioned Arc of Approach method. The method consists of two consecutive linear interpolations. In the first step, linear interpolation along the line  $PR$  and along the line  $PS$  will respectively, give the distribution function at  $lb$  and  $la$ . The corresponding expressions are:

$$f_{la}(r) = \left(\frac{f_S - f_R}{PS}\right)r + f_P, \quad (32)$$

$$f_{lb}(r) = \left(\frac{f_S - f_P}{PR}\right)r + f_P, \quad (33)$$

where  $r$  is the distance from the center. For, simplicity, its value is chosen to be  $\Delta s/2$ . In the second step, the linear interpolation is done along the arc of radius  $\Delta s/2$ . This gives the distribution function at  $l$  and  $l'$ . The expressions are given by

$$f_l = \left(\frac{f_{lb} - f_{la}}{\theta_R - \theta_S}\right)\theta + \left(\frac{f_{la}\theta_R - f_{lb}\theta_S}{\theta_R - \theta_S}\right) \quad (34)$$

Similarly, for the other side of line  $Pq$ , we have

$$f_{l'} = \left(\frac{f_{l'b} - f_{l'a}}{\theta_{R'} - \theta_{S'}}\right)\theta + \left(\frac{f_{l'a}\theta_{R'} - f_{l'b}\theta_{S'}}{\theta_{R'} - \theta_{S'}}\right). \quad (35)$$

Now, after taking moments of equation (27) with  $\psi$ , we get

$$\frac{\partial U}{\partial t} = - \sum_{all\ edges} \int_0^{\theta_{2,RS}} \int_{\theta_{1,RS}} \frac{\psi v}{2} \left[ \frac{2v\Delta t}{\Delta s} (f_P - f_l) + F_{l'P} - F_{Pl} \right] dvd\theta \quad (36)$$

Simplifying the integrand, we have

$$\frac{\partial U}{\partial t} = - \sum_{all\ edges} \int_0^{\theta_{2,RS}} \int_{\theta_{1,RS}} \psi v [\chi_P(v, \theta) f_P + \chi_S(v, \theta) f_S + \chi_R(v, \theta) f_R + \chi_{S'}(v, \theta) f_{S'} + \chi_{R'}(v, \theta) f_{R'}] dvd\theta \quad (37)$$

where

$$\begin{bmatrix} \chi_P(v, \theta) \\ \chi_S(v, \theta) \\ \chi_R(v, \theta) \\ \chi_{S'}(v, \theta) \\ \chi_{R'}(v, \theta) \end{bmatrix} = \begin{bmatrix} B - D + \psi_P(C' - A') + \psi_l(C - A) \\ A\psi_l - B \\ D - C\psi_l \\ A'\psi_P \\ -C'\psi_P \end{bmatrix} \quad (38)$$

where

$$\begin{bmatrix} A \\ B \\ C \\ D \end{bmatrix} = \begin{bmatrix} \frac{v}{2PS} \left(1 - \frac{v\Delta t}{\Delta s}\right) \frac{(\theta - \theta_R)}{\theta_S - \theta_R} \\ \frac{v}{PS} \frac{(\theta - \theta_R)}{\theta_S - \theta_R} \\ \frac{v}{2PR} \left(1 - \frac{v\Delta t}{\Delta s}\right) \frac{(\theta - \theta_S)}{\theta_S - \theta_R} \\ \frac{v}{PR} \frac{(\theta - \theta_S)}{\theta_S - \theta_R} \end{bmatrix} \quad (39)$$

and

$$\begin{bmatrix} A' \\ B' \\ C' \\ D' \end{bmatrix} = \begin{bmatrix} \frac{v}{2PS'} \left(1 - \frac{v\Delta t}{\Delta s'}\right) \frac{(\theta - \theta_{R'})}{\theta_{S'} - \theta_{R'}} \\ \frac{v}{PS'} \frac{(\theta - \theta_{R'})}{\theta_{S'} - \theta_{R'}} \\ \frac{v}{2PR'} \left(1 - \frac{v\Delta t}{\Delta s'}\right) \frac{(\theta - \theta_{S'})}{\theta_{S'} - \theta_{R'}} \\ \frac{v}{PR'} \frac{(\theta - \theta_{S'})}{\theta_{S'} - \theta_{R'}} \end{bmatrix}. \quad (40)$$

The above integral for each edge of the sum contains 25 integrals (5 distribution functions with 5 beams each) of the form

$$I = \int_0^{\infty} \int_{\theta_{1,rs}}^{\theta_{2,rs}} \psi v \times \chi(v, \theta) \times c \times \delta(v \cos \theta - u^{(1)}) \delta(v \sin \theta - u^{(2)}) dv d\theta \quad (41)$$

where  $\chi = \chi_P, \chi_S, \chi_R, \chi_{R'}$  or  $\chi_{S'}$  and other variables is as defined for equation (14). Finally, integrating it gives

$$I = \begin{cases} \phi \chi(q, \theta_0) c & \theta_{1,rs} < \theta_0 < \theta_{2,rs} \\ 0 & \text{otherwise} \end{cases} \quad (42)$$

#### 4. Results and Discussion

The scheme developed in previous section has been applied on the following test cases. The first test case is solving 2-D Burgers' Equation given by

$$\frac{\partial u}{\partial t} + \frac{\partial u^2}{\partial x} + \frac{\partial u}{\partial y} = 0. \quad (43)$$

And rest of the test case is for 2D Euler's Equations

##### 4.1. An oblique shock for 2-D Burgers' equation:

Specification (Spekreijse [45]):

Domain:  $(0,1) \times (0,1)$

Grid:  $32 \times 32, 64 \times 64$

Boundary-Conditions (Oblique Shock):

$$\left\{ \begin{array}{l} u(0, y) = 1.5 \quad 0 < y < 1 \\ u(1, y) = -0.5 \quad 0 < y < 1 \\ u(x, 0) = 1.5 - 2x \quad 0 < x < 1 \end{array} \right\} \quad (44)$$

First order results compared with KFVS(as shown in figure(4)) shows genuinely multidimensional nature of the scheme as the shock capturing is less diffusive even though shock is oblique to the grid . Second order results are shown in figure (5).

##### 4.2. Regular Shock Reflection

Specification:

Domain:  $(0,3) \times (0,1)$

Grid : Uniform  $60 \times 20, 120 \times 40$

Initial Conditions:  $(\rho, u, v, p) |_{(x,y,0)} = (1, 2.9, 0, 1/1.4)$

Boundary Conditions:

$(\rho, u, v, p) |_{(0,y,t)} = (1, 2.9, 0, 1/1.4)$

$(\rho, u, v, p) |_{(x,1,t)} = (1.69997, 2.61934, 0.50633, 1.52819)$

Dirichlet boundary condition is applied on top left boundaries. Bottom boundary is perfectly reflecting wall and right boundary is supersonic outlet.

The pressure values across the domain obtained with GINEUS are compared with KFVS (as shown in figure (6)) and it becomes clear that GINEUS has far better resolution of shock than KFVS. Similar trend can be seen in the second order comparison (figure (7)).

##### 4.3. Horizontal Slip Flow

Specification (Manna [28]):

Domain:  $(0,1) \times (0,1)$

Grid : Uniform  $40 \times 40$

Initial Condition:  $M=2$  for  $y \leq x$  and  $M=3$  for  $y > x$ .

Boundary Condition: Left boundary is supersonic inflow and top, bottom and right boundary is supersonic outflow.

To test the genuinely multidimensional nature of the scheme we are comparing the resolution of contacts aligned to the grid and it is found that there is no appreciable difference (figure (8)). In the next section oblique slip flow is compared and it is expected that the resolution of contact with GINEUS must be same in both cases.



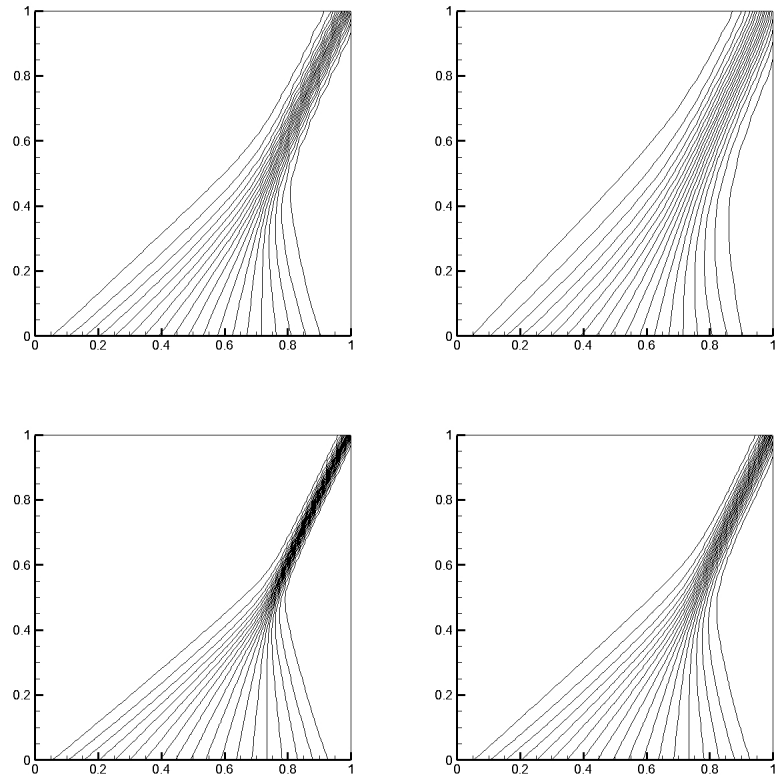


Figure 4: Contours of solution to the oblique shock test case for 2D Burger's equation by GINEUS (left) compared with KFVS (right) on  $32 \times 32$  (top) and  $64 \times 64$  (bottom) grid [I order].

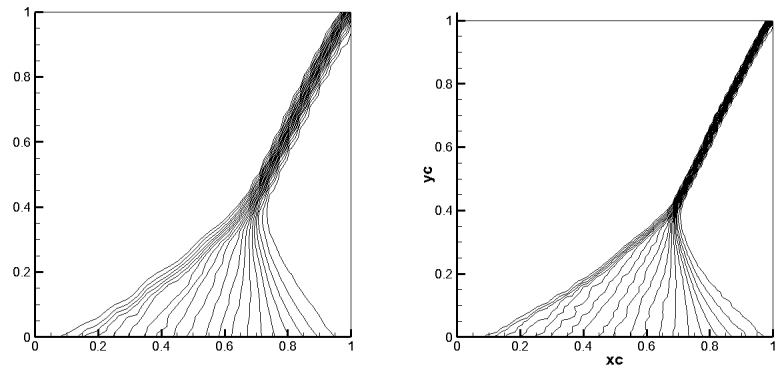


Figure 5: Contours of solution to the oblique shock test case for 2D Burger's equation by GINEUS on  $32 \times 32$  (left) and  $64 \times 64$  (right) grid [II order].

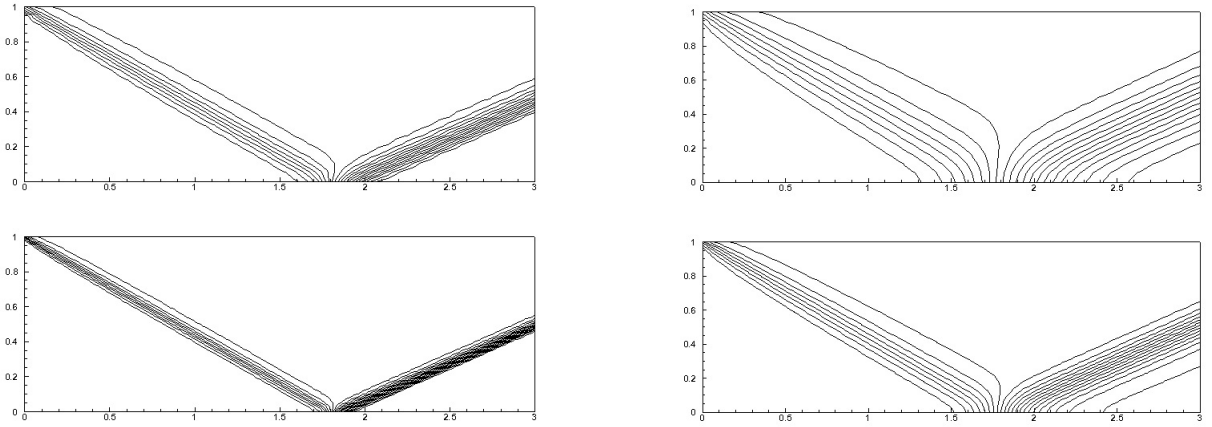


Figure 6: Pressure contours by GINEUS (left) compared with KFVS (right) for regular shock reflection in  $60 \times 20$  (top) and  $120 \times 40$  (bottom) grid [I order].

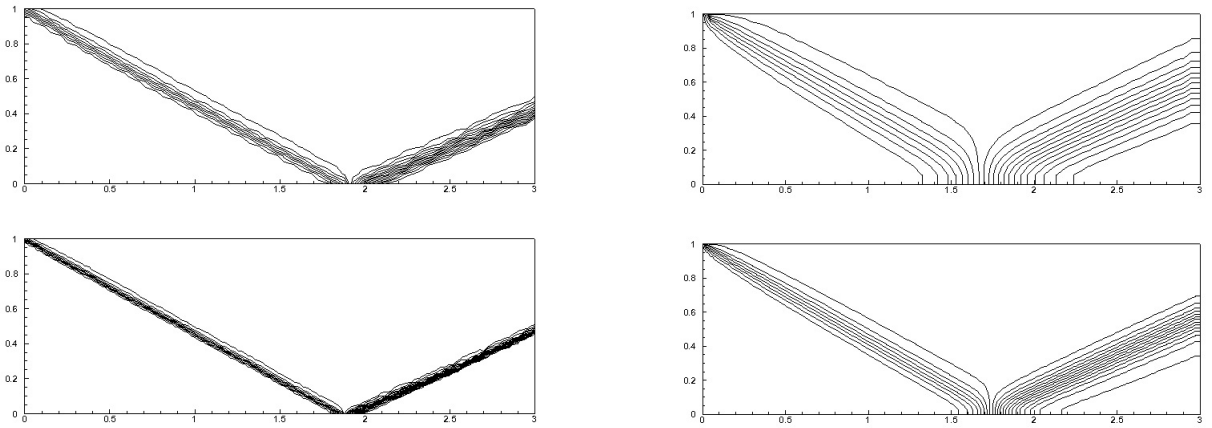


Figure 7: Pressure contours by GINEUS (left) compared with KFVS (right) for regular shock reflection in  $60 \times 20$  (top) and  $120 \times 40$  (bottom) grid [II order].

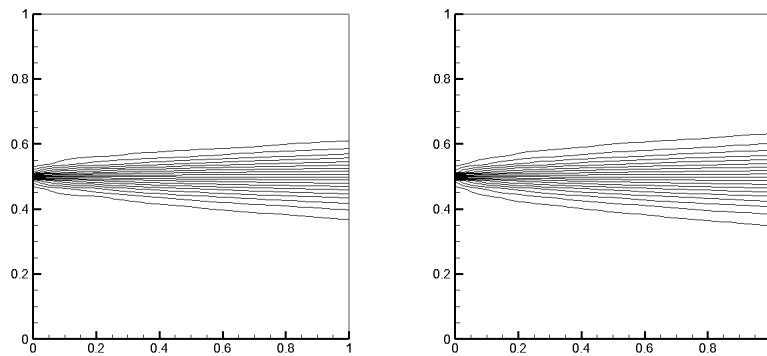


Figure 8: Mach contours for Horizontal Slip flow by GINEUS (left) and KFVS (right) on  $40 \times 40$  grid.

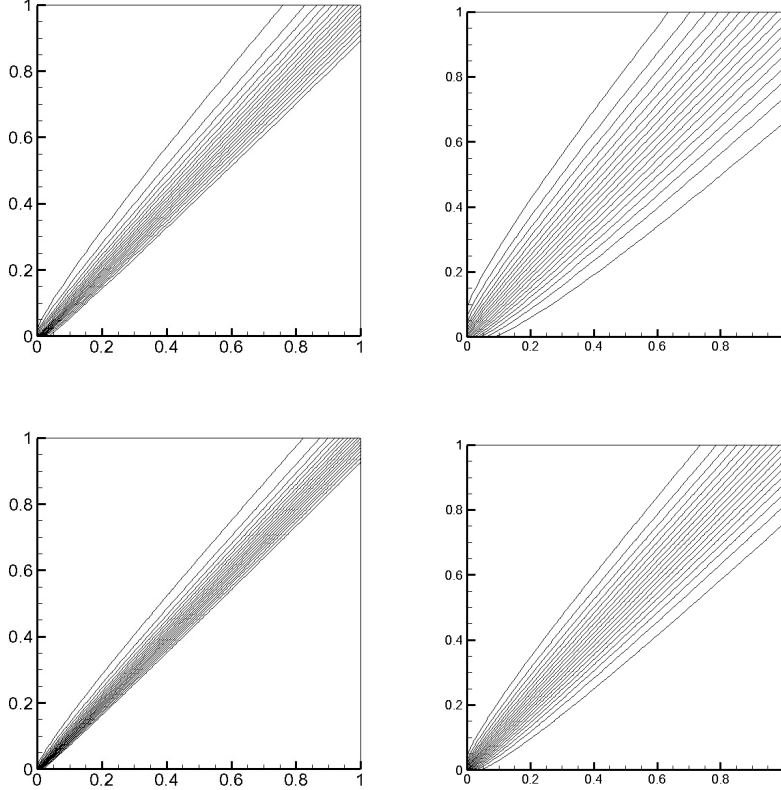


Figure 9: Mach contours by GINEUS (left) compared with KFVS (right) for oblique slip flow in  $40 \times 40$  (top) and  $80 \times 80$  (bottom) grid [1 order].

#### 4.4. Oblique Slip Flow

Specification:

Domain:  $(0,1) \times (0,1)$

Grid : Uniform  $40 \times 40$

Initial Condition:  $M=2$  for  $y \leq x$  and  $M=3$  for  $y > x$ .

Boundary Condition: Left and bottom boundary is supersonic inflow and top and right boundary is supersonic outflow.

It can be clearly seen that (figure (9)), for GINEUS, resolution of shock is similar to the horizontal slip flow whereas diffusion of contact has increased for KFVS.

#### 4.5. Supersonic Jet Interaction

Specification (Deconinck et al. [9]):

Domain:  $(0,1) \times (0,1)$

Grid : Uniform  $40 \times 40$

Initial Condition:

$$\left\{ \begin{array}{l} M_1 = 4, \rho_1 = 0.5, p_1 = 0.25 \text{ for } y > 0.5 \\ M_2 = 2.4, \rho_2 = 1.0, p_2 = 1.0 \text{ for } y < 0.5 \end{array} \right\} \quad (45)$$

Boundary Condition: Left boundary is supersonic inflow and top, bottom and right boundary is supersonic outflow.

The resolution of shock and expansion in case is much better in case of GINEUS as compared with KFVS (figure (10)). Whereas the resolution of contacts is nearly comparable because contacts are nearly alligned to the grid. This is a perfect demonstration of multidimensional feature of GINEUS. The density contours for second order extension is given in figure (11).

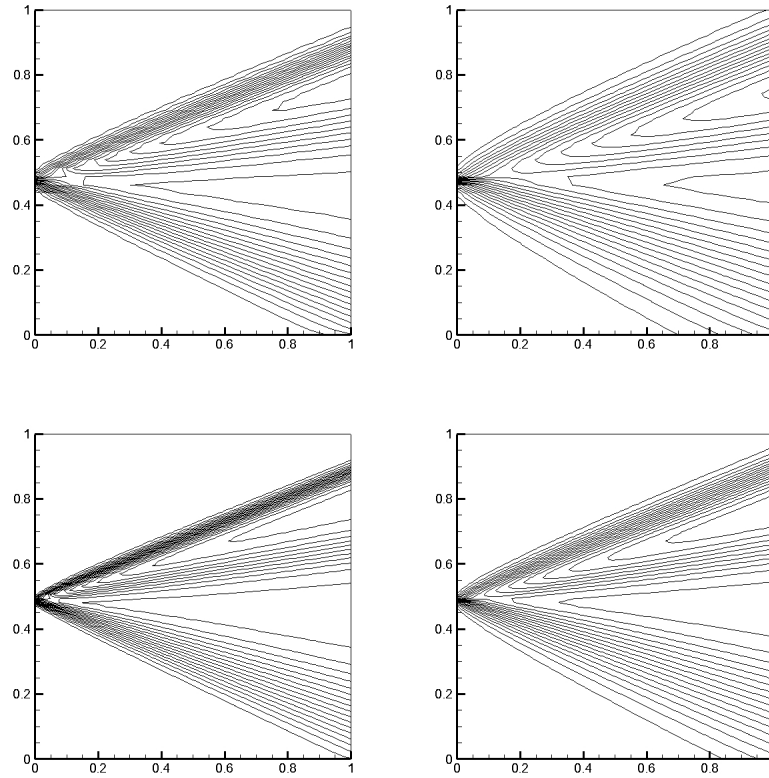


Figure 10: Density contours by GINEUS (left) compared with KFVS (right) for supersonic jet reflection on  $40 \times 40$  (top) and  $80 \times 80$  (bottom) grid [I order].

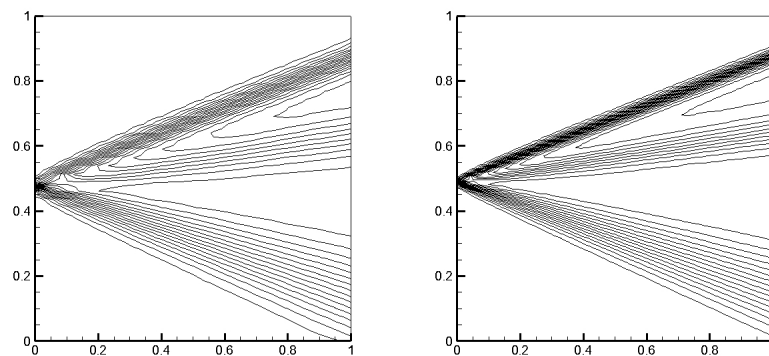


Figure 11: Density contours by GINEUS for supersonic jet reflection on  $40 \times 40$  (left) and  $80 \times 80$  (right) grid [II order].

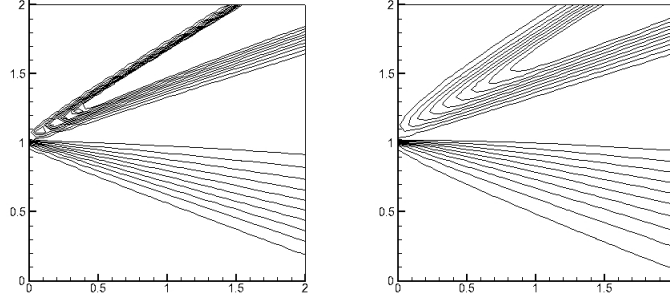


Figure 12: Density contours by GINEUS (left) compared with KFVS (right) for modified supersonic jet reflection on  $40 \times 40$  grid.

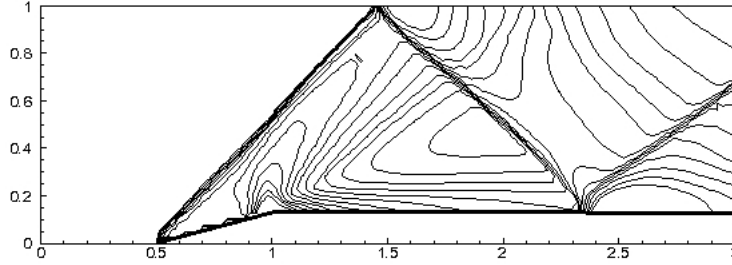


Figure 13: Mach Contours by GINEUS with I order accuracy for the flow over a ramp test case on  $120 \times 40$  grid.

#### 4.6. Modified Supersonic Jet Interaction

Specification:

Domain:  $(0,1) \times (0,1)$

Grid : Uniform  $40 \times 40$

Initial Condition:

$$\left\{ \begin{array}{l} M_1 = 4, \rho_1 = 0.5, p_1 = 0.08 \text{ for } y > 0.5 \\ M_2 = 2.8, \rho_2 = 1.0, p_2 = 1.3 \text{ for } y < 0.5 \end{array} \right\} \quad (46)$$

Boundary Condition: Left boundary is supersonic inflow and top, bottom and right boundary is supersonic outflow.

This test case is created to demonstrate improved capturing of contacts when it is not aligned to the grid.(figure 12)

#### 4.7. Supersonic flow over a Ramp

Specification (Levy et al. [23]):

Domain:  $(0,3) \times (0,1)$

Grid : Uniform  $120 \times 40$ . Since the scheme is meshless, we don't need to switch to non-cartesian grid. Instead grid points are divided into two categories: domain interior (flow region) and domain exterior. The points in the domain exterior whose adjacent point is in domain interior is taken as ghost points. The ramp starts at  $x=0.5$  and extends till  $x=1.0$  inclined at an angle of  $15^\circ$ .

Initial Condition: Mach 2 flow inside the domain.

Boundary Condition: Left boundary is supersonic inflow. Top, bottom and ramp surface is reflecting boundary. Right boundary is supersonic outflow.

Different features of the flow is brilliantly captured even with course grid of  $120 \times 40$  (figure (13)).

#### 4.8. Shock Explosion in a Box

Specification(Deiterding):

Domian:  $(0,1) \times (0,1)$

Grid : Uniform  $50 \times 50$  ,  $100 \times 100$ .

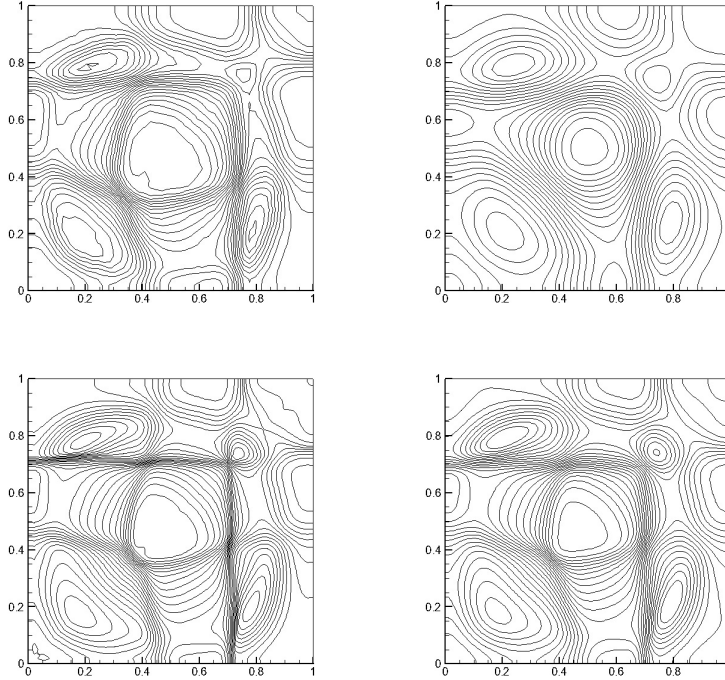


Figure 14: Density contours by GINEUS (left) compared with KFVS (right) for explosion in a box on  $50 \times 50$  (top) and  $100 \times 100$  (bottom) grid [I order].

Initial Condition: Shock bubble of radius 0.3 centered at  $(0.4, 0.4)$ . Pressure and density inside the bubble is 5 and outside it is 1. At  $t=0$ , fluid is stationary.

Boundary Condition: All boundaries are reflecting.

The initial shock fronts will expand to the boundaries and get reflected. These reflected waves will interact with each other to produce a complicated flow field. The flow is observed after  $t=0.5$ s and density contours for first order compared with KFVS can be seen in figure (14) and for second order in figure (15).

#### 4.9. Double Mach Reflection

Specification (Woodward and Colella [48]) :

Domain:  $(0, 4) \times (0, 1)$

Grid:  $240 \times 60$

Initial Condition: A shock of  $M=10$  is present at an angle of  $30^\circ$  to the  $x$ -axis, starting from  $x$ -axis at  $x=1/6$ . Density and pressure ahead of the shock is 1.4 and 1 respectively.

Boundary Condition: The intersection of top boundary with shock front moves with a speed of  $10/\cos(30^\circ)$ . Top boundary values ahead and behind the shock assumes initial values. Left boundary is supersonic inflow

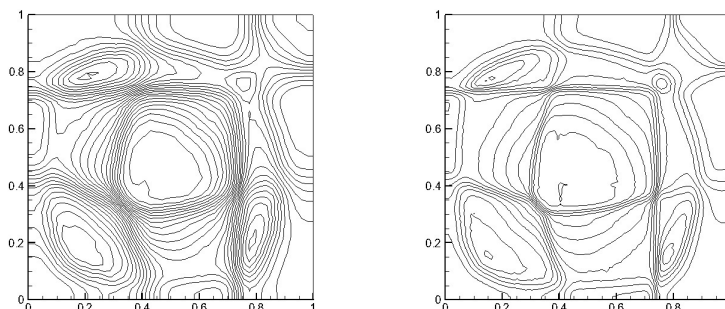


Figure 15: Density contours by GINEUS for explosion in a box on  $50 \times 50$  (left) and  $100 \times 100$  (right) grid [II order].

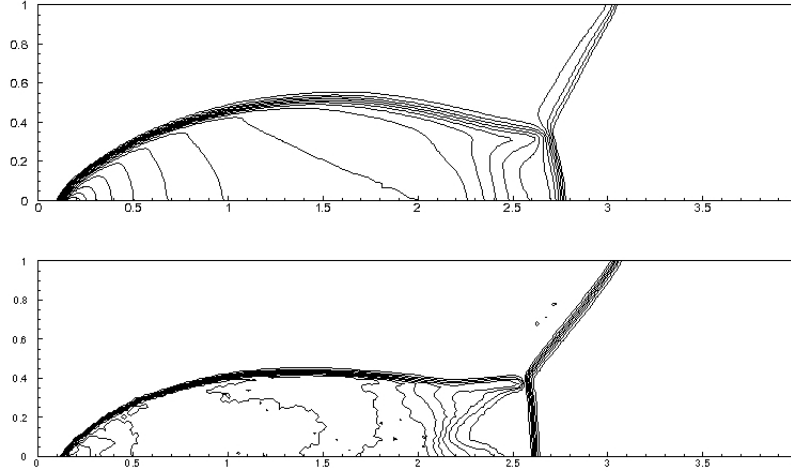


Figure 16: Pressure Contours by GINEUS having I order (top) and II order (bottom) accuracy for Double Mach Reflection on  $240 \times 60$  grid

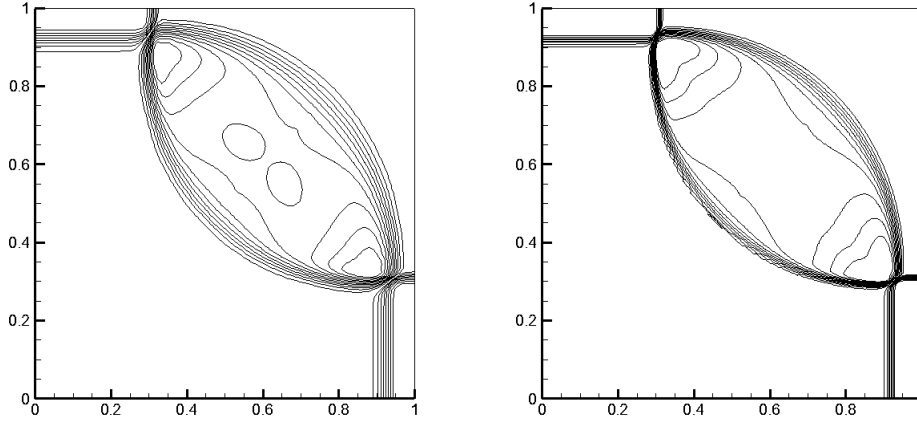


Figure 17: Density contours of GINEUS with I order accuracy for 2D Riemann test case on  $100 \times 100$  (left) and  $200 \times 200$  (right) grid

whereas right boundary is simply extrapolation from inside. The bottom boundary before  $x=1/6$  is constant initial value and for  $x>1/6$ , it is a reflecting wall.

The flow features are observed after  $t=0.2s$ . Pressure contours for the first and second order GINEUS is plotted in figure (16).

#### 4.10. 2D Riemann Problem

Specification (Liska and Wendroff [25]):

Domain:  $(0,1) \times (0,1)$

Grid:  $100 \times 100$ ,  $200 \times 200$

Initial Condition: Jump in primitive variables in 2D

$$\begin{cases} \rho = 0.5065, u_1 = 0.8939, u_2 = 0.0, p = 0.35 & \text{for } x < 0.5, y > 0.5 \\ \rho = 1.1, u_1 = 0.0, u_2 = 0.0, p = 1.1 & \text{for } x \geq 0.5, y > 0.5 \\ \rho = 1.1, u_1 = 0.8939, u_2 = 0.8939, p = 1.1 & \text{for } x < 0.5, y \leq 0.5 \\ \rho = 0.5065, u_1 = 0.0, u_2 = 0.8939, p = 0.35 & \text{for } x \geq 0.5, y \leq 0.5 \end{cases} \quad (47)$$

Boundary Condition: All the boundary values are obtained simply by extrapolating from inside. The flow is observed after  $t=0.25s$ .

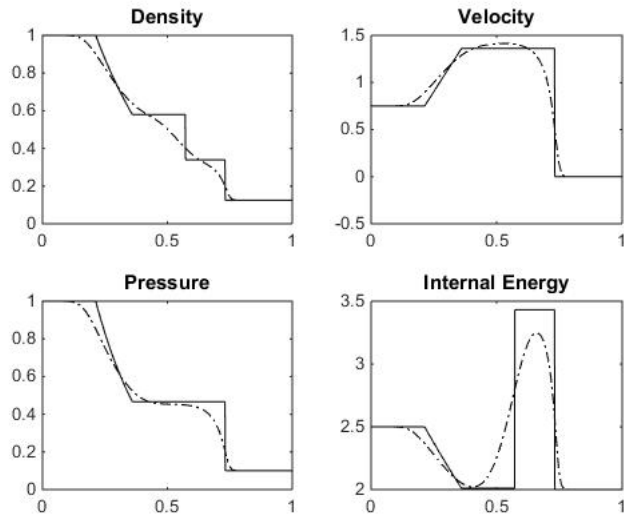


Figure 18: Torro Test case 1.

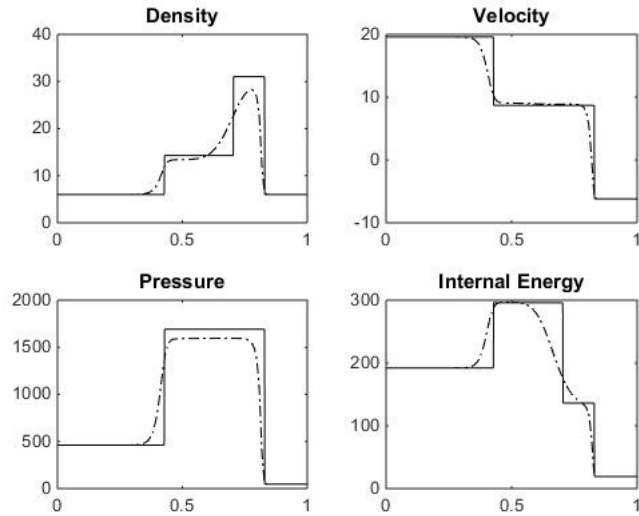


Figure 19: Torro Test case 4.

#### 4.11. Some Additional 1D Riemann Problem

The scheme is readily built to capture flow features in multidimensions but to show its robustness, this 2D formulation is used to model a 1D flow. This is done by making the domain in y-direction very small while modelling the flow in x-direction and using symmetric boundary condition for top and bottom walls. The 1D test case used is Torro's Riemann Problem (Toro [47]) and primitive variables are plotted for test case 1 and test case 4 (figure (18) and figure (19) respectively) .

## 5 Conclusion

As mentioned in the first section, present formulation is implementation of the framework with upwind method. The framework can be extended to any other finite volume, finite difference or finite element scheme. In order to obtain extra data points for the second order, we can replace 'Arc of Approach' method by second order polynomial approximation of the distribution function inside a cell, i.e.

$$f(x, y) = a_1x^2 + a_2y^2 + a_3xy + a_4x + a_5y + a_6. \quad (48)$$



Suppose that there are  $n'$  data points around the central data point. Determining the neighboring points in a mesh-less domain is itself tricky but there are established methods to resolve this issue. To calculate the coefficient  $a_i$ s, we minimize the squared error given by 49, with respect to each of  $a_i$ .

$$S = \sum_{i=0}^n (f(x_i, y_i) - f_i^{eq})^2 \quad (49)$$

Using this interpolated function, we can get the data value inside the region confined by the neighbouring points which can be used in the second order extension of the scheme.

Apart from the variations in the discretization, distribution function can also be varied. Perthame's hat function[33] or Qu, Shu and Chew's circular distribution function [36] are the possible replacements for the beams.

## References

- [1] Abgrall, R. (1993). A genuinely multidimensional riemann solver. Technical report, Institut National de Recherche en Informatique et en Automatique.
- [2] Arun, K., Kraft, M., Lukacova-Medvid'ova, M., and Prasad, P. (2009). Finite volume evolution galerkin method for hyperbolic conservation laws with spatially varying flux functions. *Journal of Computational Physics*, 228:565–590.
- [3] Arun, K. and Lukacova-Medvid'ova, M. (2013). A Characteristics Based Genuinely multidimensional discrete kinetic scheme for the euler equations. *Journal of Scientific Computing*, 55:40–64.
- [4] Balsara, D. S. (2010). Multidimensional hllc riemann solver: Application to euler and magnetohydrodynamic flows. *Journal of Computational Physics*, 229:1970–1993.
- [5] Balsara, D. S. (2014). Multidimensional riemann problem with self-similar internal structure. part i - application to hyperbolic conservation laws on structured meshes. *Journal of Computational Physics*, 277:163–200.
- [6] Balsara, D. S. and Dumbser, M. (2015). Multidimensional riemann problem with self-similar internal structure. part ii - application to hyperbolic conservation laws on unstructured meshes. *Journal of Computational Physics*, 287:269–292.
- [7] Colella, P. (1990). Multidimensional upwind methods for hyperbolic conservation laws. *Journal of Computational Physics*, 87:171–200.
- [8] Dadone, A. and Bernard, G. (1991). A rotated upwind scheme for euler equations. In *AIAA, 29th Aerospace Sciences Meeting*.
- [9] Deconinck, H., Paillere, H., Struijs, R., and Roe, P. (1993). Multidimensional upwind schemes based on fluctuation-splitting for systems of conservation laws. *Computational Mechanics*, 11:323–340.
- [10] Deiterding, R. (2015). *Blockstructured Adaptive Mesh Refinement in object-oriented C++*. AMROC.
- [11] Eppard, W. and Grossman, B. (1993). A multidimensional kinetic-based upwind solver for the euler equations. *AIAA*, 11:–.
- [12] Godunov, S. (1969). A Difference Scheme for Numerical Solution of Discontinuous Solution of Hydrodynamic Equations. *Math. Subornik*, 47:271–306.
- [13] Hirsch, C., Lacor, C., and Deconinck, H. (1987). Convection Algorithms based on a diagonalization procedure for the multidimensional Euler equations. *AIAA*, 8.
- [14] Jaisankar, S. and Rao, S. R. (2009). A Central Rankine Hugoniot Solver for Hyperbolic Conservation Laws. *Journal of Computational Physics*, 228:770–778.
- [15] Jaisankar, S. and Sheshadri, T. (2013). Directional diffusion regulator (ddr) for some numerical solvers of hyperbolic conservation laws. *Journal of Computational Physics*, 233:83–99.
- [16] Kissmann, R., Pomoell, J., and Kley, W. (2009). A central conservative scheme for general rectangular grids. *Journal of Computational Physics*, 228:2119–2131.
- [17] Kurganov, A. and Petrova, G. (2001). A third-order semidiscrete genuinely multidimensional central scheme for hyperbolic conservation laws and related problems. *Numer. Math.*, 88:683–729.
- [18] Kurganov, A. and Tadmor, E. (2000). New high-resolution central schemes for nonlinear conservation laws and convection-diffusion equations. *Journal of Computational Physics*, 160:241–282.
- [19] Lax, P. and Wendroff, B. (1960). Systems of conservation laws. *Communications in Pure and Applied Mathematics*, 13(2):217–237.
- [20] Leer, B. V. (1979). Towards the Ultimate Conservative Difference Scheme, V. a Second Order Sequel to Godunov's Method. *Journal of Computational Physics*, 32:101–136.

- [21] LeVeque, R. and Pelanti, M. (2001). A class of approximate Riemann solvers and their relation to relaxation schemes. *Journal of Computational Physics*, 172:572.
- [22] LeVeque, R. J. (1997). Wave propagation algorithms for multidimensional hyperbolic systems. *Journal of Computational Physics*, 131:327–353.
- [23] Levy, D. W., Powell, K. G., and van Leer, B. (1993). Use of a rotated riemann solver for the two-dimensional euler equations. *Journal of Computational Physics*, 106:201–214.
- [24] Liou, M.-S. (1996). A Sequel to AUSM: AUSM+. *Journal of Computational Physics*, 129:364–382.
- [25] Liska, R. and Wendroff, B. (2003). Comparison of several difference schemes in 1d and 2d Test Problems for Euler Equations. *SIAM Journal of Scientific Computation*, 25:995–1017. Unpublished.
- [26] Lukacova-Medvid’ova, M., Morton, K., and Warnecke, G. (2004). Finite volume evolution galerkin (fveg) methods for hyperbolic problems. *SIAM J. Sci. Comput.*, 26:1–30.
- [27] Lukacova-Medvid’ova, M., Saibertova, J., and Warnecke, G. (2002). Finite volume evolution galerkin methods for nonlinear hyperbolic systems. *Journal of Computational Physics*, 183:533–562.
- [28] Manna, M. (1992). A three-dimensional high resolution upwind finite volume euler solver. Technical report, von Karman Institute for Fluid Dynamics.
- [29] Mishra, S. and Tadmor, E. (2011). Constraint Preserving Schemes using Potential based Fluxes ii Genuinely Multidimensional Systems of Conservation Laws. *Journal of Numerical Analysis*, 49:1023–1045.
- [30] Osher, S. and Solomon, F. (1982). Upwind Difference Schemes fo Hyperbolic Systems of Equations. *Mathematics of Computation*, 38:339–374.
- [31] Parpia, I. and Michalek, D. (1990). A shock capturing method for multidimensional flow. In *Flight Simulation Technologies Conference*.
- [32] Parpia, I. and Michalek, D. (1992). A nearly monotone genuinely multidimensional scheme for the Euler equations. In *30th Aerospace Science Meeting*.
- [33] Perthame, B. (1991). Boltzmann Type Schemes for Gas Dynamics and Entropy Property. *SIAM Journal of Numerical Analysis*, 27:1405.
- [34] P.L.Roe (1982). *Numerical Methods for Fluid Dynamics*, chapter Fluctuations and signals – a framework for numerical evolution problems, in, pages 219–257. Academic Press.
- [35] Powell, K. G. and van Leer, B. (1989). A Genuinely Multidimensional Upwind Cell-Vertex Scheme for the Euler Equations. In *27th Aerospace Meeting*.
- [36] Qu, K., Shu, C., and Chew, Y. T. (2007). Simulation of Shock Wave Propagation with Finite Volume Lattice Boltzmann Method. *Journal of Computational Physics*, 18:447–454.
- [37] Rao, S. R. and Deshpande, S. (1991). A Genuinely Multidimensional Upwind Boltzmann Scheme for Euler Equations. Technical report, Indian Institute of Science.
- [38] Rao, S. R. and Rao, M. V. S. (2003). A simple multidimensional relaxation scheme based on characteristic and interpolation. In *16th AIAA CFD Conference*.
- [39] Razavi, S. E., Zamzamin, K., and Farzadi, A. (2008). Genuinely multidimensional characteristic-based scheme for incompressible flows. *Int. J. Numer. Meth. Fluids*, 57:929–949.
- [40] Roe, P. (1981). Approximate Riemann solvers, parameter vectors and difference schemes. *Journal of Computational Physics*, 43:357–372.
- [41] Roe, P. (1986). Discrete models for the numerical analysis of time-dependent multidimensional gas dynamics. *Journal of Computational Physics*, 63:458–476.
- [42] Roe, P. L. and Deconinck, H. (1991). *Algorithmic Trends in Computational Fluid Dynamics*, chapter Beyond the Riemann Problem Part I and II, pages 341–396. Springer and Verlag.

- [43] Rossmannith, J. A. (2008). A class of residual distribution schemes and their relation to relaxation systems. *Journal of Computational Physics*, 227:9527–9553.
- [44] Sanders, R. and Prendergast, K. (1974). The Possible Relation of the 3-kiloparsec Arm to Explosions in The Galactic Nucleus. *Astrophysical Journal*, 188:489–500.
- [45] Spekreijse, S. (1987). Multigrid Solutions to Monotone Second Order Discretizations of Hyperbolic Conservation Laws. *Mathematics of Computation*, 49:135–155.
- [46] Sweby, P. (1984). High resolution schemes using flux limiters for hyperbolic conservation laws. *SIAM J. Num. Anal.*, 21.
- [47] Toro, E. F. (2009). *Riemann Solver and Numerical Methods for Computational Fluid Dynamics*. Springer.
- [48] Woodward, P. and Colella, P. (1984). The Numerical Simulation of Two-Dimensional Fluid flow with Strong Shocks. *Journal of Computational Physics*, 54:115–173.

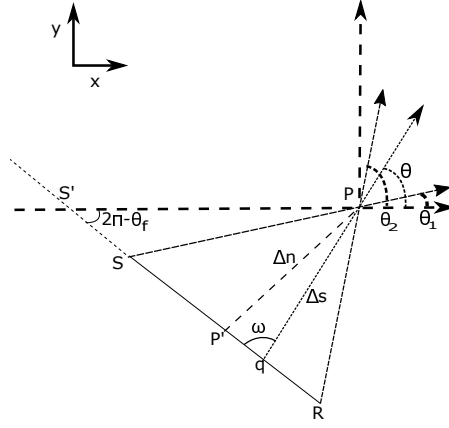


Figure A.20: Parameter Definitions when P' lies in between RS.

## Appendix A. Linear Interpolation of Distribution Function

The expression for  $f_q$  in terms of  $f_r$  and  $f_s$  can be determined using linear interpolation as:

$$f_q = k_1 r + k_2 \quad (\text{A.1})$$

Using,  $r = 0$  at  $f_q = f_s$  and  $r = SR$  at  $f_q = f_R$ , we have

$$f_q = \frac{(f_R - f_S)}{SR} r + f_S \quad (\text{A.2})$$

Now, to determine  $r$ , position of  $P'$  (point of intersection of perpendicular drawn from the center to the line  $RS$ ) has to be taken into account. They are

Appendix A.1. When  $P'$  lie on  $RS$ :

Using the figure (A.20) :

$$\angle PS'S + \angle S'PS = \angle PQP' \quad (\text{A.3})$$

or  $(2\pi - \theta_f) + \theta = \omega$ , Hence

$$\omega = \theta - \theta_f \quad (\text{A.4})$$

,

Now,

$$r = Sq = SP' - qP' \quad (\text{A.5})$$

But  $qP' = \Delta n / \tan \omega$ . Using (A.2),

$$f_q = \frac{(f_R - f_S)}{SR} \left( SP' - \frac{\Delta n}{\tan \omega} \right) + f_S \quad (\text{A.6})$$

which gives,

$$f_q = f_S \left( 1 - \frac{SP'}{SR} + \frac{\Delta n}{SR \times \tan \omega} \right) + f_R \left( \frac{SP'}{SR} - \frac{\Delta n}{SR \times \tan \omega} \right) \quad (\text{A.7})$$

so that

$$D_1 = \frac{SP'}{SR} - \frac{\Delta n}{SR \times \tan \omega} ; D_2 = 1 - \frac{SP'}{SR} + \frac{\Delta n}{SR \times \tan \omega} \quad (\text{A.8})$$

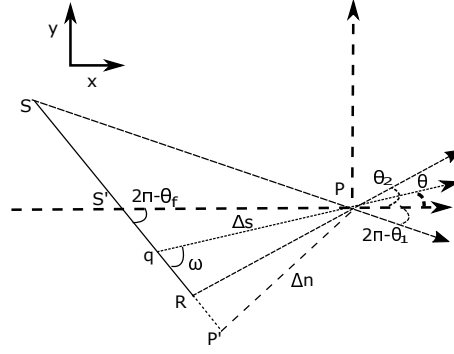


Figure A.21: Parameter Definitions when P' lies beyond R.

Appendix A.2. When P' lie beyond R:

Using the figure (A.21) :

$$\angle PS'q + \angle S'Pq = \angle PqR \quad (\text{A.9})$$

or  $(2\pi - \theta_f) + \theta = \omega$ . Hence

$$\omega = \theta - \theta_f \quad (\text{A.10})$$

Now,

$$r = Sq = SP' - qP'. \quad (\text{A.11})$$

But  $qP' = \Delta n / \tan \omega$ , hence

$$f_q = \frac{(f_R - f_S)}{SR} (SP' - \frac{\Delta n}{\tan \omega}) + f_S, \quad (\text{A.12})$$

which gives

$$f_q = f_S \left(1 - \frac{SP'}{SR} + \frac{\Delta n}{SR \times \tan \omega}\right) + f_R \left(\frac{SP'}{SR} - \frac{\Delta n}{SR \times \tan \omega}\right), \quad (\text{A.13})$$

so that

$$D_1 = \frac{SP'}{SR} - \frac{\Delta n}{SR \times \tan \omega}; \quad D_2 = 1 - \frac{SP'}{SR} + \frac{\Delta n}{SR \times \tan \omega}. \quad (\text{A.14})$$

Appendix A.3. When P' lie beyond S:

Using the figure (A.22) :

$$\angle PS'q + \angle S'Pq + \angle S'qP = \pi \quad (\text{A.15})$$

or  $(\pi - \theta_f) + \theta + \omega = \pi$ , hence

$$\omega = \theta_f - \theta. \quad (\text{A.16})$$

Now,

$$r = Sq = qP' - SP' \quad (\text{A.17})$$

But,  $qP' = \Delta n / \tan \alpha$ , hence

$$f_q = \frac{(f_R - f_S)}{SR} \left(\frac{\Delta n}{\tan \alpha} - SP'\right) + f_S \quad (\text{A.18})$$

which gives

$$f_q = f_S \left(1 + \frac{SP'}{SR} - \frac{\Delta n}{SR \times \tan \omega}\right) + f_R \left(\frac{\Delta n}{SR \times \tan \omega} - \frac{SP'}{SR}\right), \quad (\text{A.19})$$

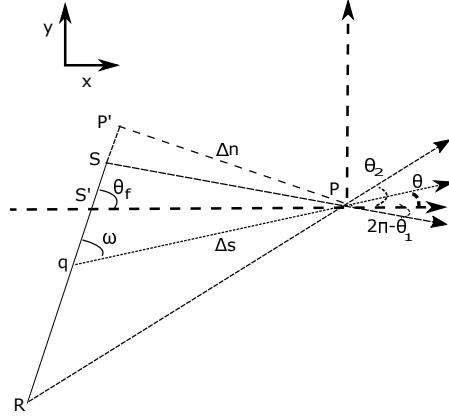


Figure A.22: Parameter Definitions when P' lies beyond S.

so that

$$D_1 = \frac{\Delta n}{SR \times \tan \omega} - \frac{SP'}{SR}; D_2 = 1 + \frac{SP'}{SR} - \frac{\Delta n}{SR \times \tan \omega}. \quad (\text{A.20})$$

## Appendix B. Replacing 2-D Maxwellian with Dirac-Delta Function

We will be comparing and matching different moments of the Maxwellian and Dirac Delta Function

The values for parameters appearing in the modified distribution function can be obtained using moment matching, i.e.,

$$\langle f^M \rangle = \rho \Rightarrow \langle f^B \rangle = a + 4b = \rho \quad (\text{B.1})$$

Similarly,

$$\langle v_1^2 f^B \rangle = au_1^2 + 4bu_1^2 + 2b \Delta u_1^2 = P + \rho u_1^2, \quad (\text{B.2})$$

$$\langle v_2^2 f^B \rangle = au_2^2 + 4bu_2^2 + 2b \Delta u_2^2 = P + \rho u_2^2, \quad (\text{B.3})$$

and

$$\langle (v_1 - u_1)^4 f^B \rangle = 2b \Delta u_1^4 = \frac{3P^2}{\rho} \quad (\text{B.4})$$

Solving the above four equations we get,  $a = \rho/3$ ,  $b = \rho/6$  and  $\Delta u_1 = \Delta u_2 = \sqrt{3P/\rho}$ .